DESCRIBING THE MECHANISM OF INSTABILITY SUPPRESSION USING A CENTRAL PILOT FLAME WITH COUPLED EXPERIMENTS AND SIMULATIONS

Jihang Li, Pennsylvania State University, University Park, PA, USA, lijihang26@gmail.com

Hyunguk Kwon, Pennsylvania State University, University Park, PA, USA, hzk78@psu.edu

Drue Seksinsky, Pennsylvania State University, University Park, PA, USA, dds82@psu.edu

Daniel Doleiden, Pennsylvania State University, University Park, PA, USA, dgd5036@psu.edu

Jacqueline O'Connor, Pennsylvania State University, University Park, PA, USA, jxo22@psu.edu

Yuan Xuan, Pennsylvania State University, University Park, PA, USA, yux19@psu.edu

Michel Akiki, Solar Turbines Incorporated, San Diego, CA, USA, akiki_michel@solarturbines.com

James Blust, Solar Turbines Incorporated, San Diego, CA, USA, blust_james_w@solarturbines.com

ABSTRACT

Pilot flames are commonly used to extend combustor operability limits and suppress combustion oscillations in low-emissions gas turbines. Combustion oscillations, a coupling between heat release rate oscillations and combustor acoustics, can arise at the operability limits of low-emissions combustors where the flame is more susceptible to perturbations. While the use of pilot flames is common in land-based gas turbine combustors, the mechanism by which they suppress instability is still unclear. In this study, we consider the impact of a central jet pilot on the stability of a swirl-stabilized flame in a variable-length, single-nozzle combustor. Previously, the pilot flame was found to suppress the instability for a range of equivalence ratios and combustor lengths. We hypothesize that combustion oscillation suppression by the pilot occurs because the pilot provides hot gases to the vortex breakdown region of the flow that recirculate and improve the static, and hence dynamic, stability of the main flame. This hypothesis is based on a series of experimental results that show that pilot efficacy is a strong function of pilot equivalence ratio but not pilot flow rate, which would indicate that the temperature of the pilot gases as well as the combustion intensity of the pilot flame play more of a role in oscillation stabilization than the length of the pilot flame relative to the main flame. Further, the pilot flame efficacy increases with pilot flame equivalence ratio until it matches the main flame equivalence ratio; at pilot equivalence ratios greater than the main equivalence ratio, the pilot flame efficacy does not change significantly with pilot equivalence ratio. To understand these results, we use large-eddy simulation to provide a detailed analysis of the flow in the region of the pilot flame and the transport of radical species in the region between the main flame and pilot flame. The

simulation, using a flamelet/progress variable-based chemistry tabulation approach and standard eddy viscosity/diffusivity turbulence closure models, provides detailed information that is inaccessible through experimental measurements.

NOMENCLATURE

f_{inst}	Instability frequency
$\dot{m}_{pilot}$	Pilot mass flowrate
r	Radial coordinate
z	Axial coordinate
C_s	Smagorinsky model constant
L_{comb}	Overall combustor length
P'	Acoustic pressure fluctuation
P_{mean}	Combustor mean pressure
Q'	Heat release rate fluctuation
μ_t	Sub-grid turbulent viscosity
ϕ_{global}	Global equivalence ratio
ϕ_{main}	Main flame equivalence ratio
ϕ_{pilot}	Pilot flame equivalence ratio
Π	Percentage of fuel diverted to pilot
Π_{air}	Percentage of air diverted to pilot

INTRODUCTION

Combustion oscillations, a coupling between flame heat release rate oscillations and acoustic fields in the combustion chamber, is a significant issue for low-emissions gas turbines [1]. In order to reduce NO_x emissions from these combustors without the use of water, combustors are operated in a fuel-lean mode, which reduces flame temperature as well as the range over which flames can operate with robust static and dynamic stability [2]. These instabilities lead to increased pollutant emissions, premature component wear, and increased potential for flame flashback or blow-off. Thus, many studies have been devoted to the understanding and mitigation of these oscillations.

Instability mitigation techniques are generally divided into active and passive categories. Active mitigation techniques aim to directly interrupt the instability cycle by modulating reactant flow on a timescale commensurate with the period of the acoustic cycle

[3,4]. Passive methods, such as fuel staging, may apply a uniform parameter change on much longer timescales to alter the acoustic response of the combustor [5]. Other passive methods reduce the sensitivity of the reactant mixing process to acoustic oscillations via passive damping [6] or alter the acoustic response of the combustor itself using acoustic damping devices [7]. Pilot flames, defined as small secondary flames in proximity to larger main flames, can be implemented in an active or passive fashion to control thermoacoustic instabilities [8–11]. Pilot flames are generally either positioned in an annular ('ring') fashion around a main flame or as a thin central torch inside a main flame. Piloting is utilized in designs by several manufacturers of land-based gas turbine engines [12–14].

The presence of a pilot flame affects both the static and dynamic stability of the main flame. Static stability refers to the limits of flame-holding and the range of conditions between flame flashback and blowoff. Dynamic stability refers to thermoacoustic instability, where acoustic oscillations couple with the flame to drive large-scale heat release rate oscillations. Near lean blow-off (LBO) conditions, pilot flames enhance static stability by providing a consistent source of heat and radical chemical species near the base of the flame, thus promoting flame anchoring [13,15–18]. Under conditions where the main flame is already anchored, generation of heat and radical species by the pilot flame may also enhance the dynamic stability of the flame for very similar to reasons to enhancing the static stability. Lean flames, like those used in modern low-emissions gas turbine combustors, are highly susceptible to external perturbations because quantities like heat release rate and flame speed are highly sensitive to changes in inflow conditions near the lean blowout limit; as such, they are more likely to be thermoacoustically unstable than stoichiometric flames [19].

An example of pilot flames used to enhance dynamic stability is the combined experimental and large eddy simulation (LES) work of Sengissen et al. [20], who demonstrated that piloting prevents the formation of precessing vortex core (PVC) formation, stabilizing the main flame. A pilot flame may also weaken main flame-vortex interaction, as shown by Lee et al. [21]. However, previous results from the current experiment considered in this study showed that the presence of a pilot flame can have a destabilizing effect in certain cases [22].

Various studies of other types of burners with a central jet have also been conducted. Gupta et al. [23] used a double-concentric premixed burner consisting of a central nozzle with two swirled outer annuli to study the effects of radial swirl distribution. They observed the formation of a thin but intense reaction zone when the annuli were counter-swirled, along with non-symmetric temperature fluctuation. Russ et al. [24] established a physical model for frequency-dependent flame dynamics of steady-state premixed flames to which experimental data from a lean premixed (LP) and lean premixed pre-vaporized (LPP) burner was supplied. This burner consisted of a swirled central pilot lance surrounded by a concentric adjustable swirled LP/LPP main flame. Meier et al. [25] used a turbulent diffusion burner for confined swirled natural gas flames. This burner enabled probability density function measurements of temperature, mixture fraction, and presence of major chemical species to be taken, with the aim of validating commonly available models.

In the current experiment, the amplitude of the instability increases, decreases, or stays the same with the addition of the pilot flame depending on the operating condition, pilot flow rate, and pilot equivalence ratio. Previous studies by Li et al. [22] in this same experimental configuration presented a two-dimensional stability map relating acoustic pressure fluctuation to percentage of total fuel flow diverted to the pilot flame (Π) and global equivalence ratio (ϕ_{global}). A pilot fuel flow percentage sweep was conducted across one of the stability boundaries of the stability map to study the abrupt increase in acoustic pressure fluctuation associated with the boundary. Without piloting, the main flame was not anchored and heat release primarily occurred in the corner recirculation zone. Addition of piloting caused the flame to propagate upstream towards the centerbody, shifting heat release to an inner shear layer. This structural change in flame anchoring exposed the flame to strong vortices, causing instability.

One of the main questions that arose from this previous work was the mechanism by which the central pilot flame stabilizes the main flame in the cases where it is effective. In these initial studies, the pilot flame air flow rate was held constant and only the equivalence ratio varied, keeping the overall power of the combustor constant. In the current study, we vary both the pilot equivalence ratio and flow rate in order to understand the relative impact of the thermal versus fluid mechanic changes that occur with the addition of pilot. We find that instability suppression is much more sensitive to pilot equivalence ratio than flow rate. To understand why, we have used high-fidelity large-eddy simulation to probe the pilot region and quantify the interaction between the pilot and main flame at several key conditions. The simulations suggest that the amount of heat and radical species transferred to the base of the main flame from the pilot flame is more a function of pilot equivalence ratio, ϕ_{pilot}, and less a function of pilot mass flow rate, $\dot{m}_{pilot}$. This is determined by analyzing the temperature and species distribution, in addition to the reverse flow strength, in the region near the base of the main and pilot flames where hot, radical-filled fluid from the pilot flame can be recirculated to the main flame, “back supporting” the main flame.

The remainder of this paper is organized as follows. We first introduce the experiment as well as the simulation. Next, we describe the experimental study, which spans a large range of pilot equivalence ratios and flow rates, to quantify the sensitivity of pilot efficacy to both parameters. Finally, we use the simulations at four key conditions to understand the relative roles of pilot equivalence ratio and flow rate on instability suppression. We conclude by discussing the implications of these findings on pilot design for instability suppression.

EXPERIMENTAL OVERVIEW AND METHODS

Experimental configuration

Experimental measurements were taken in a single-nozzle model combustor with a swirl-stabilized, lean-premixed flame burning natural gas and air. The configuration of the experiment is shown in Figure 1, which identifies the inlet section, the optically-accessible quartz combustor, and the tunable exhaust section. The main-flame air is metered using a Sierra 570S thermal-mass flow meter. The main-flame fuel is metered with a Teledyne Hastings HFM-301 flowmeter and injected in the swirler. The main-flame mixture is electrically preheated to 250 °C. The pilot-flame air and the pilot-flame fuel are metered with two Teledyne Hastings HFM-D-301A flowmeters and are preheated to the same temperature as the main-flame mixture ahead of the injector. Given that main and pilot air and fuel streams are controlled independently, the flow rate and equivalence ratio of the premixed pilot can be varied independently of the main flame.

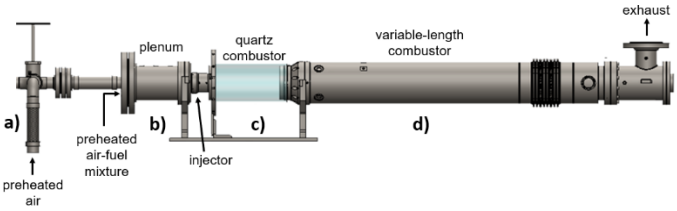

Figure 1: The experimental apparatus showing: a) the inlet section; b) the plenum; c) the quartz combustor; and d) the metallic variable-length combustor.

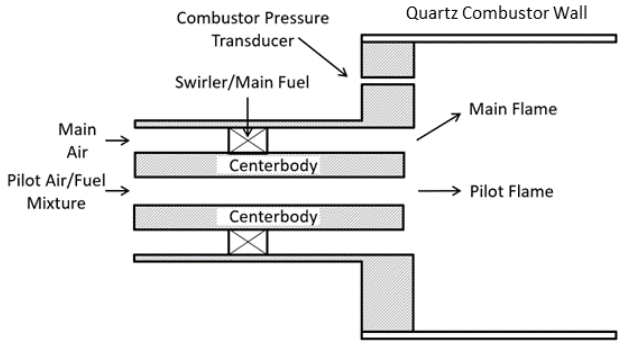

Figure 2: Schematic of the nozzle showing the flow paths of the pilot mixture, the swirled main mixture, and the locations of the main and pilot flames.

Figure 2 shows a schematic of the injector. The main air flows through an annular pass with a swirler at a bulk flow velocity of 40 m/s. Fuel is injected through holes in the swirler vanes, making the main mixture “technically premixed.” The pilot fuel and air, which are premixed ahead of the injector, flows through the center of the injector and into the combustion chamber in an axial jet. This injector configuration is representative of a range of industrial hardware used in modern gas turbine engines and so it is expected that the results from this work are applicable to a variety of injector technologies. The quartz combustor liner seen in Figure 1 and Figure 2 is 15 cm in

diameter and 30.5 cm long, and allows the entire structure of the main and pilot flames to be accessed optically. Downstream of the quartz combustor section is a metal variable-length exhaust section that allows for the system to be acoustically tuned. The exhaust has an inner diameter of 12.3 cm and is terminated by a water-cooled plug that can be moved using a stepper motor-controlled traverser system (Isel-Automation), resulting in a length variation of 63.5-149.9 cm in increments of 0.25 cm.

Diagnostics

The instability levels are monitored with water-cooled dynamic pressure transducers (PCB) located in the dump plane and in the main-air passage of the injector; two transducers are mounted in the injector in order to monitor the acoustic velocity fluctuation levels using the two-microphone method [26]. Pressure is sampled at a rate of 8192 Hz.

The structure of the flame is captured with CH* chemiluminescence images using a Photron Fastcam SA4 camera coupled to an Invisible Vision UVi intensifier with a bandpass filter centered at 432 nm. This combination allows images of the entire structure of the main and pilot flames to be captured with a frame rate of 4000 frames per second, an exposure time of 200 μs, and a resolution of 27.4 pixels per centimeter.

Data analysis

The stability of the combustor is characterized quantitatively by determining the root-mean-squared (RMS) level of the acoustic pressure fluctuation at the dump plane (P'_{RMS}) within a ±10 Hz band centered about the instability frequency for each operating condition. The combustor is considered to be unstable when the normalized pressure RMS level (P'_{RMS}/P_{mean}) exceeds 0.01.

To pre-process the flame images, a median filter in the spatial domain is applied to the background-subtracted images to reduce the speckle noise. To better illustrate the spatial distribution of the chemiluminescence emission, the filtered line-of-sight images are deconvoluted using the Inverse Abel transform [27]. This process generates the distribution of the chemiluminescence emission in a 2-D plane through the centerline. Note that the algorithm assumes an axisymmetric flame, so the upper and lower halves of the flame images are averaged beforehand to eliminate any asymmetry about the centerline.

SIMULATION

Numerical models

In this work, the Simcenter STAR-CCM+ software is used to perform the LES of the single-nozzle model combustor. In these simulations, large turbulent eddies are resolved and the effects of sub-grid scale (SGS) eddies are modelled by sub-grid turbulent viscosity, μ_t; the Smagorinsky model with constant eddy viscosity is used [28].

The Flamelet Generated Manifold (FGM) model [29], developed to approximate complex combustion reactions with a reduced computational cost, is used in this work. In the FGM model, all of the thermochemical quantities (e.g., temperature, mixture density, and species concentrations) involved in the detailed chemical kinetics are mapped to a flamelet-based database, which are retrieved during CFD simulations. The thermochemical data is tabulated as a function of mixture fraction, heat loss ratio, and progress variable. The progress variable is defined in this work as the sum of the mass fractions of CO and CO_2. The FGM table is generated within Star-CCM+ based on solutions of 0-D, constant-pressure reactor simulations using the GRI-Mech 3.0 chemical model [30].

Geometry and simulation setup

An unstructured polyhedral mesh consisting of approximately 16.7 million cells is generated for the model combustor shown in Figure 1 using the automated mesh generation tool in Star-CCM+; mesh convergence studies were performed to ensure accuracy in the flame shape. Fuel and air are injected the same way in the model as in the experiment: technically premixed in the main flow and fully premixed in the pilot flow. A steady-state Reynolds-Averaged Navier-Stokes (RANS) simulation is first performed to obtain an initial solution with artificial ignitors to initialize flame stabilization. After that, the ignitors are removed and LES is performed starting from the steady-state RANS solution until a statistically-stationary state is reached. All the LES simulations are carried out with a time-step of 10^{-4} s and 10 inner iterations to achieve appropriate convergence using the residuals. Wall heat losses are accounted for in the simulations by setting a temperature of 600 K at the air-cooled centerbody tip, 900 K at the air-cooled combustor liner, and 400 K at the water-cooled dump plane and combustor plug. These temperatures are estimated based on measurements and best practices in simulations of similar combustors.

Both the RANS simulations and LES are performed under the low-Mach number limit, which does not resolve the acoustic oscillations in the system. While some of the experimental conditions considered in this study are thermoacoustically unstable, indicating that acoustic oscillations are present and interacting with the flame, previous work in this combustor at similar conditions has shown that the time-averaged flame shape is not a strong function of the amplitude of acoustic oscillation for most instability modes. While the oscillations certainly change quantities like the flame brush thickness, the quantities of interest for the comparison to CFD – flame stabilization location and time-averaged flame angle – do not change between stable and unstable conditions. Hence, to test our hypothesis about the bulk transport of gases through recirculation from the pilot flame to the main flame, it is not necessary to capture the details of the thermoacoustic oscillations given the much higher computational cost of a simulation with acoustics.

RESULTS AND DISCUSSION

Test matrix

As described in Li et al. [22], the combustor is thermoacoustically unstable at a length of 711.2 mm and an equivalence ratio of 0.6 when no pilot flame is present. At this condition, the instability is the first longitudinal mode of the combustor at a frequency of 169 Hz and instability amplitude of P'/P_{mean}=1.31%; this is the only tonal mode in the combustor at this combustor length. The instability can be suppressed by increasing the pilot fuel to 6.5% of the total fuel flow rate, while keeping the global equivalence ratio constant. At this global equivalence ratio, there are two other instability modes of the combustor at combustor lengths of 1016 mm and 1371.6 mm. We do not detail the results at these conditions in this paper, but the results are similar in terms of instability suppression sensitivity to pilot equivalence ratio and mass flow rate.

Table 1 shows the test matrix for this study. In all tests, the main air and main fuel flow rates are held constant with an equivalence ratio of 0.6; the main air and main fuel flow rates are not varied so as to isolate the effect of the pilot on the behavior of the system. Pilot equivalence ratio is varied from 0.2 to 1.0 in increments of 0.05, and pilot mixture flow rate is varied from 0 to 0.38 kg/min at 11 different flow rates. The equivalence ratio and flow rate are varied independently of each other in order to understand the relative impact of equivalence ratio versus flow rate on the pilot's ability to suppress the instability. At a given flow rate, variation of the pilot equivalence ratio changes the temperature of the pilot and its thermal impact on the central recirculation zone. At a given equivalence ratio, variation of the pilot flow rate changes the fluid-mechanic influence of the pilot by changing the penetration of the pilot jet without changing the jet temperature. It is expected that though the expansion across the flame changes with equivalence ratio, the pilot jet flow rate will have a larger influence on the flow structure in the recirculation zone as the initial momentum of the jet changes.

Table 1: Test matrix

Main-flame equivalence ratio (ϕ_{main})	0.6
Combustor length (L_{comb})	711.2 mm
Air inlet temperature (T_{in})	250° C
Main-flame air velocity	40 m/s
Pilot Flame Equivalence Ratio (ϕ_{pilot})	0.2 – 1.0
Pilot Mixture Flow Rate ($\dot{m}_{pilot}$)	0-0.38 kg/min

Figure 3 shows an example variation in operating conditions to illustrate the efficacy of the pilot at suppressing the instability. In these figures, the y-axis is normalized RMS pressure fluctuation amplitude percentage, where the RMS is normalized by the mean combustor pressure. The x-axes show the variation in a number of critical parameters. In Figure 3a, the pilot equivalence ratio is varied

by changing the fuel flow rate of the pilot, which also changes the ratio of the fuel mass flow rate of the pilot to the fuel mass flow rate of the main. In Figure 3b, the equivalence ratio of the pilot is varied by changing the pilot air flow rate, where now the ratio of the pilot air flow rate and main air flow rate is shown. The red symbol with the red arrow in both plots has the same main equivalence ratio and pilot equivalence ratio, arrived at in the middle of two different variations. In both cases, the instability is suppressed as the pilot equivalence ratio increases regardless of how the equivalence ratio is varied – with variations in pilot fuel or air mass flow rate.

To further understand the role of pilot equivalence ratio vs. flow rate, the two quantities are varied independently, as shown in Figure 4. In this figure, normalized pressure fluctuation RMS is plotted against the mass flow rate of the pilot mixture at several different pilot equivalent ratios. The operating condition with neither pilot fuel nor pilot air, indicated by the horizontal dashed line, is used as the baseline condition.

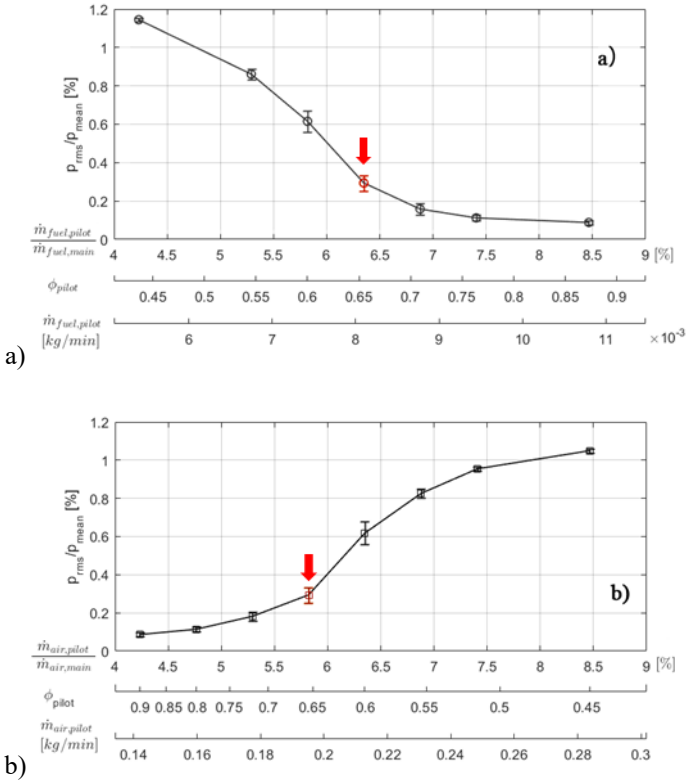

Figure 3. RMS pressure with a) varying pilot fuel flow rate and b) varying pilot air flow rate.

Figure 4 shows a few important results. First, instability suppression is achieved with higher equivalence ratio pilots. This result suggests that the extra heat added by the pilot flame supports the dynamic stability of the main flame. On the other hand, the addition of pilot with low equivalence ratio can actually exacerbate the instability. It is interesting that the dividing line between the stabilization and destabilization effects lies approximately at ϕ_{pilot} = 0.55, which is close to the equivalence ratio of the main flame (ϕ_{main}=0.6). This

likely implies that the efficacy of the pilot flame may be primarily determined by its ability to heat up or cool down the recirculation zone, whose temperature is mainly determined by the equivalence ratio of the main flame. The recirculation zone plays an important role in the flame's static stability, as it provides back support for the main flame in the high-shear region of the annular jet [31].

Second, for sufficiently high pilot equivalence ratio, ϕ_{pilot} = 0.7 and above, very small flow rates can have significant instability suppression effects. This result implies that it is the temperature of the pilot flame, but not the total amount of heat it provides, that determines the instability characteristics. Finally, as the pilot flow rate further increases, the instability magnitude is insensitive to pilot flow rate. In cases where the pilot reduces the instability amplitude, the change in pilot efficacy with pilot flow rate is very small. For example, at ϕ_{pilot} = 0.7 and 1.0, where $\phi_{pilot} > \phi_{main}$, the instability amplitude does not change at all with pilot flow rate above 0.06 kg/min. At lower equivalence ratios such as ϕ_{pilot} = 0.55 and 0.6, increasing the pilot flow rate does not significantly change the instability amplitude, either. This observation is unexpected because the flame at the baseline condition, being a transitional state between stability and instability, is expected to be sensitive to operating condition changes.

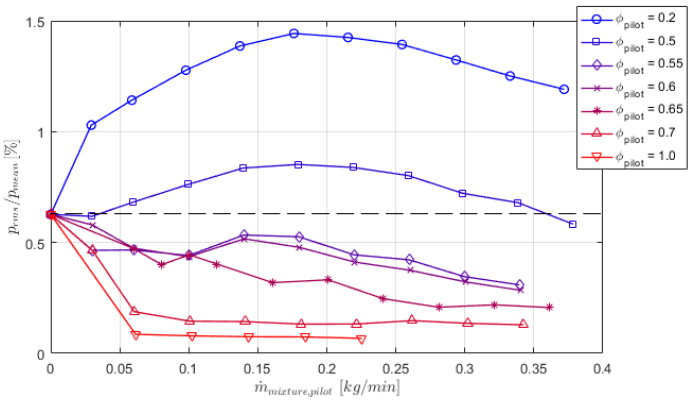

Figure 4. RMS pressure with varying pilot mixture flow rate at various pilot equivalence ratios.

The sensitivity of the oscillation to ϕ_{pilot} and the relative insensitivity to $\dot{m}_{pilot}$ are further illustrated in Figure 5, in which all data points collected in the study are plotted versus pilot equivalence ratio. Although the variation of the pilot mixture flow rate is a factor of 12 times between the highest and the lowest values, the pressure fluctuation amplitude is largely only dependent on pilot equivalence ratio.

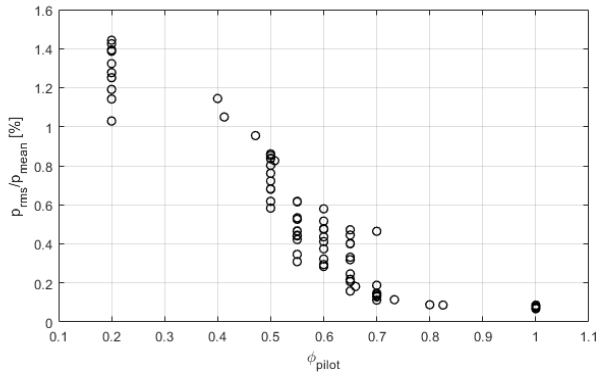

Figure 5. Scatter plot of RMS pressure vs pilot equivalence ratio for all conditions.

This result has been further confirmed by looking at data from other, very different types of tests with this same injector. Figure 6 shows the instability amplitude as a function of ϕ_{pilot}/ϕ_{main} for a variety of different operating conditions. In this figure only, the global equivalence ratio is kept constant for each data set (as shown in the legend), as are the flow rates of both main air and pilot air, such that the total thermal power of the flame is constant as ϕ_{pilot}/ϕ_{main} is varied. These data were obtained at the same preheat temperature as those described in Table 1, but at different combustor lengths. Despite the differences in main flame equivalence ratio and combustor length, the trend in pilot efficacy is still the same – the pilot flame is effective at suppressing the instability when $\phi_{pilot} > \phi_{main}$ and as the pilot equivalence ratio increases beyond that point, the instability amplitude is not significantly affected.

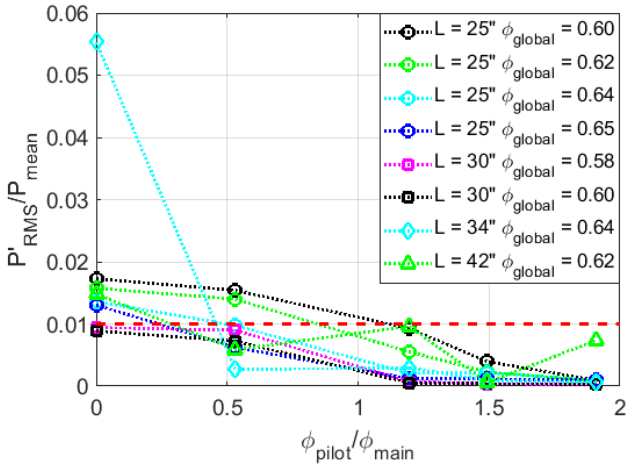

Figure 6. Instability amplitude as a function of ϕ_{pilot}/ϕ_{main} for a range of combustor lengths and global equivalence ratios in tests where global equivalence ratio is held constant. Red dotted line is the instability criterion (P'_{RMS}/P_{mean}=1%).

Impact of equivalence ratio and flow rate on flow/flame structure

Figure 7 shows the time-averaged deconvoluted images of four typical flames with various $\dot{m}_{pilot}$ and ϕ_{pilot}, in which Figure 7a is the baseline case with no pilot flow. The top of the images shows the experimental measurements of CH* chemiluminescence and the bottom of the images shows the CH distribution from the simulations. We recognize that CH* and CH distributions will not be the same, but this comparison is sufficient to understand the trends in the flame shape with variations in equivalence ratio and pilot flow rate, as well as capture the basic flame structure.

By comparing the experimental images in Figure 7a and Figure 7b, it can be observed that as an extremely lean pilot (ϕ_{pilot} = 0.2) is added, the time-averaged flame emission becomes more distributed. This is due to the fact that the case in Figure 7b has a higher pressure fluctuation amplitude and hence more flame motion. In these cases, the flame resides in both the inner shear layer and corner recirculation zone, forming an "M" flame. On the contrary, when a richer pilot (ϕ_{pilot} = 0.7) is introduced, the time-averaged flame becomes more compact and concentrated, as shown in Figure 7c. This is an indication of a more stable flame. Moreover, when the flame brush in the inner shear layer reaches the combustor liner, it mainly propagates downstream, which renders the main flame closer to a "V" flame. In the simulations, the main and pilot flames are predicted to be located slightly further downstream as compared to the measurements. However, the simulation result qualitatively captures the impact of pilot equivalence ratio and flow rate on flame shape.

These results show that the flame structure, and therefore, the instability characteristics of the main flame, are greatly influenced by the pilot equivalence ratio. This is not true for the pilot flow rate. As Figure 7c and Figure 7d show, even if the pilot flow rate is increased by a factor of three, the structure of the main flame is unaltered. To understand this effect, the structure of the pilot flame under various conditions is examined.

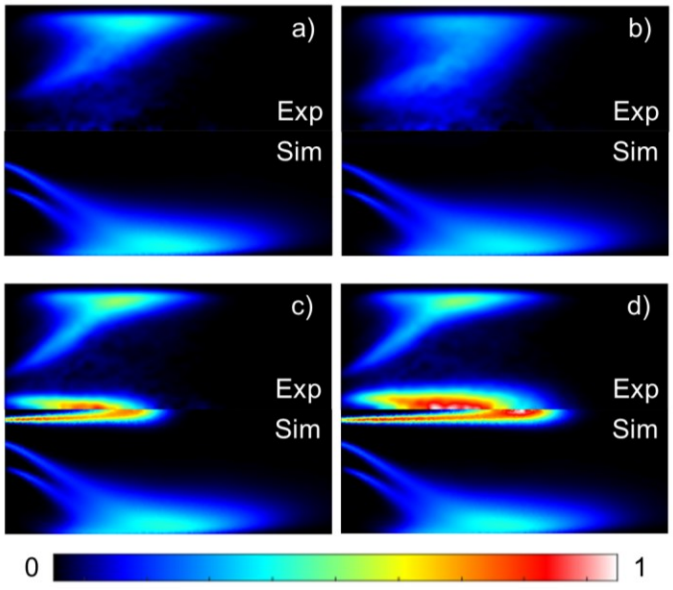

Figure 7. Time-averaged deconvoluted images of the flames at a) $\dot{m}_{pilot}$ = 0 kg/min, b) $\dot{m}_{pilot}$ = 0.1 kg/min, ϕ_{pilot} = 0.2, c) $\dot{m}_{pilot}$ = 0.1 kg/min, ϕ_{pilot} = 0.7, and d) $\dot{m}_{pilot}$ = 0.3 kg/min, ϕ_{pilot} = 0.7.

Figure 8 shows the time-averaged pilot flame length with varying pilot flow rates and pilot equivalence ratio for all the experimental cases and two simulation cases. Here, the pilot flame length is defined as the distance from the dump plane to the location where 95% of the pilot emission is contained in between. In the simulations, the pilot flame length for the two test cases with ϕ_{pilot} = 0.7 is determined in the same way as the measurements (star symbols in Figure 8). The simulation results overpredict the pilot flame length by 1% for $\dot{m}_{pilot}$ = 0.1 kg/min, ϕ_{pilot} = 0.7 and by 9% for $\dot{m}_{pilot}$ = 0.3 kg/min, ϕ_{pilot} = 0.7, which is quite a good agreement. Additionally, the simulations qualitatively predict the experimentally-observed trend that a higher pilot flow rate leads to a longer pilot flame.

It can be observed that the pilot flame length, and hence its extent of influence on the recirculation zone, is less a function of equivalence ratio and more a function of flow rate. Despite that, instability suppression is a stronger function of equivalence ratio. This result implies that the penetrating distance of the pilot flame, if exceeding a certain threshold, does not influence the instability. It is likely the upstream portion of the pilot, anchored near the nozzle, that impacts the main flame and hence the stabilizing effect – the pilot flame does not become substantially more effective as the pilot length increases.

On the contrary, when a richer pilot (ϕ_{pilot} = 0.7) is introduced, the time-averaged flame becomes more compact and concentrated, as shown in Figure 7c. This is an indication of a more stable flame. Moreover, when the flame brush in the inner shear layer reaches the wall, it mainly propagates downstream, which renders the main flame closer to a “V” flame. These results lead us to hypothesize that the pilot flame acts to suppress instability by enhancing the static stability of the main flame. This enhanced static stability is driven by the recirculation of hot products from the pilot flame into the zone between the pilot- and main-flame attachment points. A pilot flame with a lower equivalence ratio than the main will cool this region, whereas a pilot flame with an equivalence ratio higher than the main flame heats this region, enhancing stability.

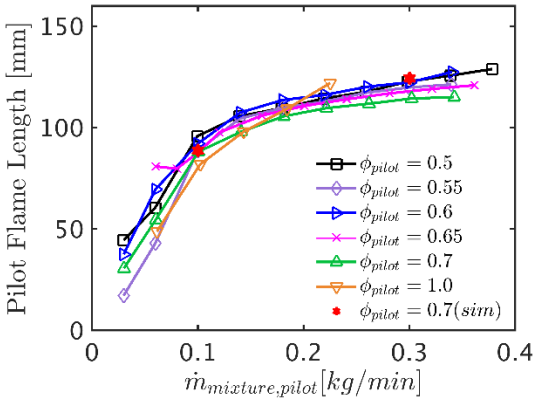

Figure 8. Time-averaged pilot flame length with varying pilot mixture flow rates flames at ϕ_{pilot} = 0.5, 0.55, 0.6, 0.65, 0.7 and 1.0.

In order to understand the trends in pilot efficacy in suppressing combustion instability, a detailed analysis of the flow in the region of the pilot flame and the transport of heat and radical species in the region between the main flame and pilot flame is required. Figure 9 shows the time-averaged axial velocity component with streamlines constructed based on the time-averaged flow field (top images) and the time-averaged temperature (bottom images) of the four flames from the simulation.

The axial velocity component plots indicate that both the corner recirculation zone and the inner recirculation zone at the base of the main flame generated by the main fuel/air mixture jet are well captured in the simulations. The structure of the recirculation zone changes somewhat with the addition of the pilot jet, resulting in a sort of "double-bubble" structure due to the different velocity boundary condition along the centerline of the flow. Figure 9b-d show that the flow structures in the inner recirculation region are qualitatively similar for the various pilot flow rate and equivalence ratios investigated.

The temperature plots show that temperature of the inner recirculation zone is influenced much more significantly by the pilot flame equivalence ratio than its flow rate. When a richer pilot (ϕ_{pilot} = 0.7) is introduced, the temperature in the inner recirculation zone is slightly higher as compared to the baseline case (no pilot). The difference in temperature with the addition of the pilot flame is small because the difference in equivalence ratio between the main flame (ϕ_{main} = 0.6) and the pilot flame (ϕ_{pilot} = 0.7) is small.

Piloting with a lean flame (ϕ_{pilot} = 0.2) significantly reduces the temperature in the inner recirculation zone. The difference in temperature in this region is both a result of the thermochemical state of the fluid as well as the flow in the region between the pilot and the main jet. First, the product temperature of the pilot flame gases is significantly less than that of the main flame products as a result of the difference in equivalence ratio. In the case without the pilot flame, the lack of pilot flame creates a stagnant zone along the centerline where hot gases can reside longer; the streamlines in the baseline case near the pilot jet exit are random and the velocity is

low, indicative of high residence times. As such, the hotter gases from the ϕ_{main} = 0.6 main flow are able to stagnate along the centerline region, whereas the cooler cases from the ϕ_{pilot} = 0.2 have more momentum as a result of the pilot jet flow.

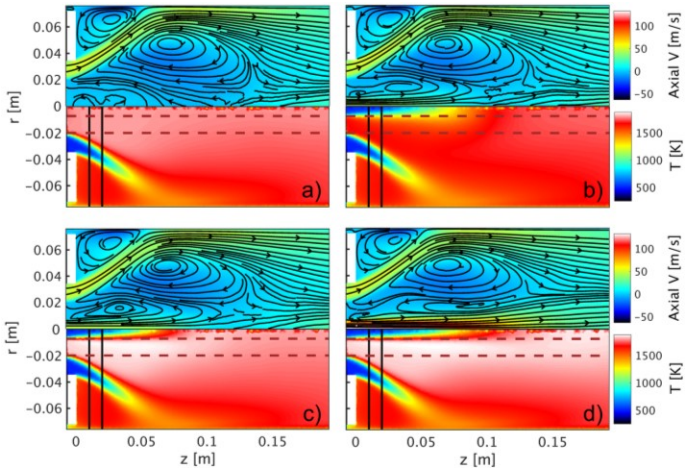

Figure 9. Time-averaged axial velocity and temperature at a) $\dot{m}_{pilot}$ = 0 kg/min, b) $\dot{m}_{pilot}$ = 0.1 kg/min, ϕ_{pilot} = 0.2, c) $\dot{m}_{pilot}$ = 0.1 kg/min, ϕ_{pilot} = 0.7, and d) $\dot{m}_{pilot}$ = 0.3 kg/min, ϕ_{pilot} = 0.7. The gap region between main and pilot flame is marked by two horizontal lines. Two vertical lines indicate the radial cuts at z = 0.01 and 0.02 m.

To further analyze the flow pattern in the inner recirculation zone and test the hypothesis that the inner recirculation zone transports hot, radical-filled gases from the higher equivalence ratio pilot to stabilize the main flame, the probability density function (PDF) of the axial velocity component at an axial location of z = 0.01 m (the left vertical line in Figure 9) is plotted at three different radial locations in Figure 10. Analyzing the axial velocity at this z = 0.01 m line indicates whether fluid is being transported towards (negative axial velocities) or away from (positive axial velocities) the base of the main flame on an instantaneous basis. If the PDF has more area under the curve below zero, then more fluid is being transported to the base, whereas a greater area under the curve above zero would indicate that fluid is being transported away from the main flame.

Near the pilot flame (r = 0.01 m and 0.015 m), the probability of positive and negative axial velocities is balanced in all of the flame cases except $\dot{m}_{pilot}$ = 0.3 kg/min and ϕ_{pilot} = 0.7. Closer to the main flame (r = 0.02 m), the probability of negative axial velocity increases, especially in the cases of high pilot flame equivalence ratio, which provides stronger transport of heat and radicals to the main flame anchoring region and consequently promotes instability suppression.

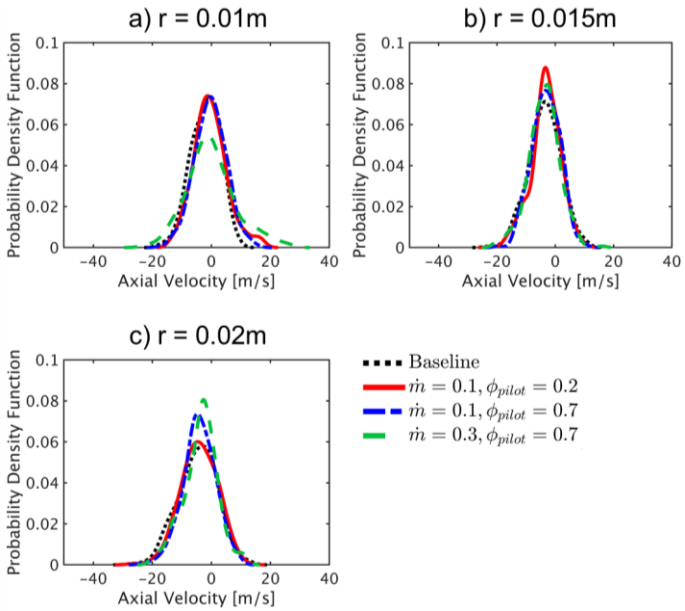

Figure 10. Probability density function (PDF) of axial velocity at z = 0.01 m with varying radical location. a) r = 0.01 m, b) r = 0.015 m, and c) r = 0.02 m.

To quantify the thermal effects of pilot flame equivalence ratio and flow rate, temperatures along the radial direction are plotted at z = 0.01 m and 0.02 m (the two dotted lines in Figure 9) in Figure 11a and Figure 11b. The gap region in the inner recirculation zone between the main and pilot flame is marked by two dotted vertical lines in Figure 11. Piloting with a higher ϕ_{pilot} compared to the main flame is shown to slightly increase the temperature in the gap region (approximately 50 K for ϕ_{pilot} = 0.7). On the other hand, the gap region temperature is reduced by up to 600 K in the leaner pilot case (ϕ_{pilot} = 0.2). Time-averaged mole fraction of OH along the same radial cuts is plotted to quantify the transfer of radicals between the main and pilot flame in Figure 11c and Figure 11d. Here, the two flames with ϕ_{pilot} = 0.7 have a similar level of OH in the gap region, which is higher than that of the baseline flame. However, the lean pilot flame case (ϕ_{pilot} = 0.2) has a reduced concentration of OH in the gap region as compared to the baseline case. Similar results have been found for other radicals important for flame stabilization, such as H and HCO. These results demonstrate that a lower ϕ_{pilot} compared to that of the main flame generally leads to weaker flame anchoring, as observed in experiments (see Figure 7), due to reduced temperature and radical concentrations at the base of the flame since the pilot flame acts as a heat and radical sink, which may make the main flame more susceptible to instabilities.

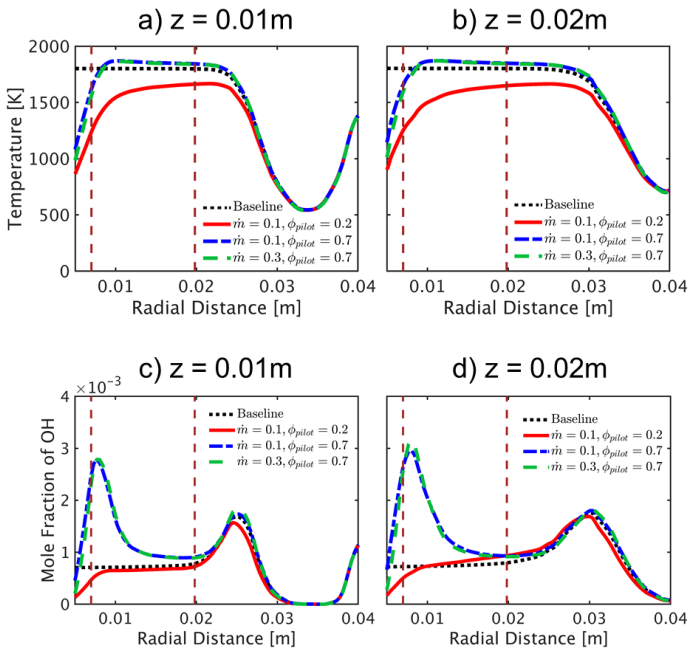

Figure 11. Radial plots of a-b) temperature and c-d) mole fraction of OH at z = 0.01 m and z = 0.02 m. The gap region between main and pilot flame is marked by two vertical dashed lines.

Our results are also consistent with previous studies of flames in different configurations. The presence of hot gas on the products side of the flame is typically referred to as "back support" for the flame. Work in both opposed-flow [32–36] and Bunsen [37,38] flame configurations shows that back support helps to insulate the flame, allowing higher intensity burning by reducing heat loss. Work by Coriton et al. [35] showed using both simulation and several species diagnostics in experiments that the thermal and chemical composition of the back support impacts the burning intensity of the main flame. In particular, their results show that back-support temperature dramatically affect the ability of the main flame to re-ignite after local turbulence-induced extinction, particularly in lean flames. Modeling indicated that the inability to ignite is the result of heat loss from the main flame to the cooler back support region. This situation mirrors the present flame configuration as the pilot flame can either drive heat addition (where $\phi_{pilot} > \phi_{main}$), or heat loss (where $\phi_{pilot} < \phi_{main}$), thereby affecting the strength of the stabilization point and its ability to resist extinction in the presence of high levels of fluid mechanical strain.

In more realistic flame configurations, like the swirl-stabilized flame investigated here, back support comes in the form of either products in the corner recirculation zones (back supporting the outer branch of the main flame) or from a central recirculation zone and pilot, if one is present. The role of recirculation on flame stabilization was investigated by Foley et al. [39] in a swirl-stabilized flame. Using an asymmetric OPPDIF simulation like the experiment by Coriton et al. [35], the back support was shown to extend the extinction

limits of the flame. This same lesson can be applied to the stabilization of the flame in this experiment, where a pilot flame with at least the same product gas temperature as the main flame provides better flame stabilization, and hence better dynamic stability characteristics.

CONCLUSION

In this study, we have used both experiments and simulations to understand how a pilot flame is able to suppress thermoacoustic instability. Experiments in a single-nozzle combustor with a central jet pilot show that the instability amplitude is relatively insensitive to pilot mass flow rate over a small flow rate threshold value, but highly sensitive to the pilot equivalence ratio. In particular, the pilot increases in efficacy as its equivalence ratio increases until it is equal with that of the main flame; further increase of the pilot flame equivalence ratio does not impact thermoacoustic instability as greatly. Based on these experimental results, we hypothesize that the pilot flame acts to suppress thermoacoustic instability by providing heat and radical species to the base of the main flame, through the action of recirculation in the vortex breakdown bubble. This additional back support of the main flame enhances its static stability and hence its dynamic stability as well. This work confirms and explains what has been seen in field experience that pilot flames can be an effective way to suppress thermoacoustic instability.

The CFD results show qualitative agreement with the experimentally-observed trends; in particular, flame shape and pilot flame length trends match well between experiment and simulation. The simulations provide quantitative insight into the instability suppression mechanism by simultaneously considering the velocity field, temperature field, and radical species distributions. It is shown that a richer pilot flame leads to a stronger recirculation region, with higher temperature and radicals transported from the pilot flame, whereas a leaner pilot flame decreases the temperature in the region of the main-flame stabilization at the centerbody and hence weakens its flame-holding capability.

The results provide useful insights into the design of the pilot flame system. In modern lean-premixed gas turbines, secondary flames can be an undesirable contributor to NO_x emission [12,40]. To reduce the NO_x emission generated by the pilot flame, either the pilot flame temperature or the total thermal power of the pilot flame has to be reduced. This study has demonstrated that the pilot equivalence ratio should be kept above a certain level to ensure a satisfying instability suppression ability. This study has also demonstrated that a low pilot flow rate of a mixture slightly richer than the main flame can contribute substantially to pilot efficacy without significantly increasing NO_x. The NO_x emission may thus be significantly reduced while still achieving effective instability suppression.

One other insight from the simulation results indicates that the action of recirculation, a result of the high levels of swirl from the main jet, must be able to overcome the aerodynamic and thermal expansion forces from the pilot flame. The results in this work may

not have been the same for a flow with lower swirl, and hence weaker central recirculation. As such, the pilot flame and the main swirl should be designed in concert to ensure that the thermochemical benefit from the pilot flame is able to reliably back support the main flame at its attachment point.

ACKNOWLEDGEMENTS

The authors are grateful for the financial support provided by the U.S. Department of Energy University Turbine Systems Research Program Grant DE-FE0031806 under contract monitor Mark Freeman and Solar Turbines Incorporated under program monitor Dave Voss. Computations for this research were performed on the Pennsylvania State University's Institute for Computational and Data Sciences' Roar supercomputer. The authors also wish to acknowledge the contributions of Dr. Dom Santavicca and Dr. Stephen Peluso to the experimental component of this work.

REFERENCES

[1] Lieuwen, T. C., and Yang, V., 2005, *Combustion Instabilities in Gas Turbine Engines: Operational Experience, Fundamental Mechanisms, and Modeling*, American Institute of Aeronautics and Astronautics, Reston, VA.

[2] McDonell, V., 2016, "Lean Combustion in Gas Turbines," *Lean Combustion*, D. Dunn-Rankin, and P. Therkelsen, eds., Academic Press, London, UK, pp. 147–201.

[3] McManus, K. R., Poinsot, T., and Candel, S. M., 1993, "A Review of Active Control of Combustion Instabilities," Prog. Energy Combust. Sci., **19**(1), pp. 1–29.

[4] Annaswamy, A. M., and Ghoniem, A. F., 2002, "Active Control of Combustion Instability: Theory and Practice," IEEE Control Syst. Mag., **22**(6), pp. 37–54.

[5] Zinn, B. T., and Lieuwen, T. C., 2005, "Combustion Instabilities: Basic Concepts," *Combustion Instabilities in Gas Turbine Engines: Operational Experience, Fundamental Mechanisms, and Modeling*, T.C. Lieuwen, and V. Yang, eds., American Institute of Aeronautics and Astronautics, Reston, VA, pp. 3–26.

[6] Scarinci, T., Freeman, C., and Day, I., 2004, "Passive Control of Combustion Instability in a Low Emissions Aeroderivative Gas Turbine," *Turbo Expo: Power for Land, Sea, and Air*, Vienna, Austria.

[7] Richards, G. A., Straub, D. L., and Robey, E. H., 2003, "Passive Control of Combustion Dynamics in Stationary Gas Turbines," J. Propuls. Power, **19**(5), pp. 795–810.

[8] Albrecht, P., Bade, S., Lacarelle, A., Paschereit, C. O., and Gutmark, E., 2010, "Instability Control by Premixed Pilot Flames,"

J. Eng. Gas Turbines Power, **132**(4), p. 041501.

[9] Seume, J. R., Vortmeyer, N., Krause, W., Hermann, J., Hantschk, C.-C., Zangl, P., Gleis, S., Vortmeyer, D., and Orthmann, A., 1998, "Application of Active Combustion Instability Control to a Heavy Duty Gas Turbine," J. Eng. Gas Turbines Power, **120**(4), pp. 721–726.

[10] Li, C., Li, S., Cheng, X., and Zhu, M., 2018, "Measurements and Modeling of the Dynamic Response of a Pilot Stabilized Premixed Flame Under Dual-Input Perturbation," J. Eng. Gas Turbines Power, **140**(12), p. 121502.

[11] Oztarlik, G., Selle, L., Poinsot, T., and Schuller, T., 2020, "Suppression of Instabilities of Swirled Premixed Flames with Minimal Secondary Hydrogen Injection," Combust. Flame, **214**, pp. 266–276.

[12] Davis, L. B., and Black, S. H., 1995, "Dry Low NOx Combustion Systems for GE Heavy-Duty Gas Turbines," *PowerGen Conference*, pp. 57–68.

[13] Subash, A. A., Collin, R., Aldén, M., Kundu, A., and Klingmann, J., 2017, "Experimental Investigation of the Influence of Burner Geometry on Flame Characteristics at a Dry Low Emission Industrial Prototype Burner at Atmospheric Pressure Conditions," *Turbo Expo: Power for Land, Sea, and Air*, Charlotte, NC.

[14] Smith, K. O., Rawlins, D. C., and Steele, R. C., 2000, "Developments in Dry Low Emissions Systems," *International Pipeline Conference*, American Society of Mechanical Engineers, p. V002T09A010.

[15] Albrecht, P., Speck, S., Schimek, S., Bauermeister, F., Gutmark, E., and Paschereit, O., 2007, "Lean Blowout Control Using an Auxiliary Premixed Flame in a Swirl-Stabilized Combustor," *43rd AIAA/ASME/SAE/ASEE Joint Propulsion Conference & Exhibit*, Cincinatti, OH.

[16] Shanbhogue, S., Shin, D.-H., Hemchandra, S., Plaks, D., and Lieuwen, T., 2009, "Flame-Sheet Dynamics of Bluff-Body Stabilized Flames during Longitudinal Acoustic Forcing," Proc. Combust. Inst., **32**(2), pp. 1787–1794.

[17] De, S., Mondal, P., Sardar, G. M., Bokhtiar, R. Bin, Bhattacharya, A., Mukhopadhyay, A., and Sen, S., 2019, "Control of Lean Blowout in Partially Premixed Swirl-Stabilized Combustor Using a Fuel Rich Central Pilot Configuration," *ASME 2019 Gas Turbine India Conference*, Chennai, Tamil Nadu India.

[18] Subash, A. A., Collin, R., Aldén, M., Kundu, A., and Klingmann, J., 2017, "Investigation of Hydrogen Enriched Methane Flame in a Dry Low Emission Industrial Prototype Burner at Atmospheric Pressure Conditions," *Turbo Expo: Power for Land, Sea, and Air*, Charlotte, NC.

[19] O'Connor, J., Hemchandra, S., and Lieuwen, T., 2016, "Combustion Instabilities in Lean Premixed Systems," *Lean Combustion: Technology and Control: Second Edition*, D. Dunn-Rankin, and P. Therkelsen, eds., Academic Press, London, UK, pp. 231–259.

[20] Sengissen, A. X., Van Kampen, J. F., Huls, R. A., Stoffels, G. G. M., Kok, J. B. W., and Poinsot, T. J., 2007, "LES and Experimental Studies of Cold and Reacting Flow in a Swirled Partially Premixed Burner with and without Fuel Modulation," Combust. Flame, **150**(1–2), pp. 40–53.

[21] Lee, J. G., Kim, K., and Santavicca, D. A., 2000, "Effect of Injection Location on the Effectiveness of an Active Control System Using Secondary Fuel Injection," Proc. Combust. Inst., **28**(1), pp. 739–746.

[22] Li, J., Peluso, S., Quay, B., Santavicca, D., Blust, J., and Srinivasan, R., 2017, "Effect of Pilot Flame on Flame Macrostructure and Combustion Instability," *Turbo Expo: Power for Land, Sea, and Air*, Charlotte, NC.

[23] Gupta, A. K., Lewis, M. J., and Daurer, M., 2001, "Swirl Effects on Combustion Characteristics of Premixed Flames," J. Eng. Gas Turbines Power, **123**(3), pp. 619–626.

[24] Russ, M., Meyer, A., and Büchner, H., 2007, "Scaling Thermo-Acoustic Characteristics of LP and LPP Swirl Flames," *Turbo Expo: Power for Land, Sea, and Air*, Montreal, Canada.

[25] Meier, W., Keck, O., Noll, B., Kunz, O., and Stricker, W., 2000, "Investigations in the TECFLAM Swirling Diffusion Flame: Laser Raman Measurements and CFD Calculations," Appl. Phys. B, **71**(5), pp. 725–731.

[26] Åbom, M., and Bodén, H., 1988, "Error Analysis of Two-microphone Measurements in Ducts with Flow," J. Acoust. Soc. Am., **83**(6), pp. 2429–2438.

[27] Alvarez, R., Rodero, A., and Quintero, M. C., 2002, "An Abel Inversion Method for Radially Resolved Measurements in the Axial Injection Torch," Spectrochim. Acta Part B At. Spectrosc., **57**(11), pp. 1665–1680.

[28] Smagorinsky, J., 1963, "General Circulation Experiments with the Primitive Equations: I. The Basic Experiment," Mon. Weather Rev., **91**(3), pp. 99–164.

[29] Pierce, C. D., and Moin, P., 2004, "Progress-Variable Approach for Large-Eddy Simulation of Non-Premixed Turbulent Combustion," J. Fluid Mech., **504**, p. 73.

[30] Smith, G. P., Golden, D. M., Frenklach, M., Moriarty, N. W., Eiteneer, B., Goldenberg, M., Bowman, C. T., Hanson, R. K., Song, S., and Gardiner Jr, W. C., 1999, "GRI 3.0 Mechanism, Version 3.0 7/30/99," Gas Res. Institute, Chicago, IL. http//combustion. berkeley. edu/gri-mech.

[31] Shanbhogue, S. J., Sanusi, Y. S., Taamallah, S., Habib, M. A., Mokheimer, E. M. A., and Ghoniem, A. F., 2016, "Flame Macrostructures, Combustion Instability and Extinction Strain Scaling in Swirl-Stabilized Premixed CH4/H2 Combustion," Combust. Flame, **163**, pp. 494–507.

[32] Coriton, B., Frank, J. H., and Gomez, A., 2016, "Interaction of Turbulent Premixed Flames with Combustion Products: Role of

Stoichiometry," Combust. Flame, **170**, pp. 37–52.

[33] Coppola, G., Coriton, B., and Gomez, A., 2009, "Highly Turbulent Counterflow Flames: A Laboratory Scale Benchmark for Practical Systems," Combust. Flame, **156**(9), pp. 1834–1843.

[34] Coriton, B., Smooke, M. D., and Gomez, A., 2010, "Effect of the Composition of the Hot Product Stream in the Quasi-Steady Extinction of Strained Premixed Flames," Combust. Flame, **157**(11), pp. 2155–2164.

[35] Coriton, B., Frank, J. H., and Gomez, A., 2013, "Effects of Strain Rate, Turbulence, Reactant Stoichiometry and Heat Losses on the Interaction of Turbulent Premixed Flames with Stoichiometric Counterflowing Combustion Products," Combust. Flame, **160**(11), pp. 2442–2456.

[36] Mastorakos, E., Taylor, A., and Whitelaw, J. H., 1995, "Extinction of Turbulent Counterflow Flames with Reactants Diluted by Hot Products," Combust. Flame, **102**(1–2), pp. 101–114.

[37] Skiba, A., Wabel, T., Carter, C. D., Hammack, S., Temme, J., and Driscoll, J., 2018, "Premixed Flames Subjected to Extreme Levels of Turbulence Part I: Flame Structure and a New Measured Regime Diagramitle," Combust. Flame, **189**, pp. 407–432.

[38] Tyagi, A., Boxx, I., Peluso, S., and O'Connor, J., 2019, "Statistics and Topology of Local Flame–Flame Interactions in Turbulent Flames," Combust. Flame, **203**.

[39] Foley, C., Chterev, I., Noble, B., Seitzman, J., and Lieuwen, T., 2017, "Shear Layer Flame Stabilization Sensitivities in a Swirling Flow," Int. J. Spray Combust. Dyn., **9**(1), pp. 3–18.

[40] Steele, R. C., Cowell, L. H., Cannon, S. M., and Smith, C. E., 2000, "Passive Control of Combustion Instability in Lean Premixed Combustors," J. Eng. Gas Turbines Power, **122**(3), pp. 412–419.